Article

Global population profile of tropical cyclone exposure from 2002 to 2019

https://doi.org/10.1038/s41586-023-06963-z

Received: 24 April 2023

Accepted: 12 December 2023

Published online: 20 December 2023

Check for updates

Renzhi Jing[1,2], Sam Heft-Neal[3], Daniel R. Chavas[4], Max Griswold[5], Zetianyu Wang[5], Aaron Clark-Ginsberg[5], Debarati Guha-Sapir[6,7], Eran Bendavid[1,2,8]✉ & Zachary Wagner[5]✉

Tropical cyclones have far-reaching impacts on livelihoods and population health that often persist years after the event[1–4]. Characterizing the demographic and socioeconomic profile and the vulnerabilities of exposed populations is essential to assess health and other risks associated with future tropical cyclone events[5]. Estimates of exposure to tropical cyclones are often regional rather than global[6] and do not consider population vulnerabilities[7]. Here we combine spatially resolved annual demographic estimates with tropical cyclone wind fields estimates to construct a global profile of the populations exposed to tropical cyclones between 2002 and 2019. We find that approximately 560 million people are exposed yearly and that the number of people exposed has increased across all cyclone intensities over the study period. The age distribution of those exposed has shifted away from children (less than 5 years old) and towards older people (more than 60 years old) in recent years compared with the early 2000s. Populations exposed to tropical cyclones are more socioeconomically deprived than those unexposed within the same country, and this relationship is more pronounced for people exposed to higher-intensity storms. By characterizing the patterns and vulnerabilities of exposed populations, our results can help identify mitigation strategies and assess the global burden and future risks of tropical cyclones.

Health risks owing to substantial natural hazards such as tropical cyclones are a central concern of climate science and public health[1–4,8]. Notable tropical cyclones, such as Hurricane Katrina and Hurricane Maria, affect regional mortality and population health, both directly and indirectly, and for many years after the event[9,10]. Fundamental to understanding the population-health hazards of tropical cyclones is characterizing the populations exposed to these storms: the number of people experiencing tropical cyclones over time, the demographic composition of the populations and the vulnerabilities of those populations. As such, the United Nations 'Sendai Framework for Disaster Risk Reduction' notes that understanding the current and historical distributions of population exposure to tropical cyclones is a key input for policy prioritization to protect vulnerable populations[5]. This paper aims to use the best available data and methods to characterize the populations exposed to tropical cyclones. In doing so, we address questions about the evolving risks of tropical cyclones, the vulnerabilities of exposed populations and the relative contributions of population growth and climate in shaping tropical cyclone exposure.

When tropical cyclones pass over populated regions, the combination of high winds, low-pressure systems, heavy rainfalls and storm surges can lead to large-scale destruction and increased risk of mortality and diseases[11,12]. There are concerns that these harmful effects could be more widespread in the future as sea temperature rises and population vulnerability increases[2,13]. Tropical cyclone exposure may be more consequential in areas with fewer resources, which are generally less equipped to effectively mitigate the impacts of storms[10,14]. Despite the importance of identifying populations vulnerable to tropical cyclones, the demographic structure and socioeconomic status of exposed populations remain unclear. Furthermore, the trade-offs between the economic opportunities offered by coastal access and the increased risk of destructive tropical cyclones make it ambiguous whether exposed populations are more or less economically vulnerable than those unexposed[15]. The relative demographic composition of groups particularly susceptible to impacts from tropical cyclone exposure, such as children and the elderly, is also unknown[16,17].

Previous studies on global population exposure to tropical cyclones have provided partial insights. First, disaster databases widely used in policy formulation and disaster research[18–20], such as EM-DAT[21], include only limited demographic information and may fail to capture the impact of frequent, smaller, yet still destructive, events. Second, traditional parametric wind models used to simulate tropical cyclone exposure did not account for asymmetry in wind speed induced by land features. Third, previous work has used relatively low-resolution population data, limiting the scope for assessing demographic patterns in exposure. Studies by Peduzzi et al.[22] and Geiger et al.[7] provide the fullest available accounts of global tropical cyclone exposure, but rely on older wind models and provide only limited characterizations of the populations exposed beyond the total counts. A detailed population profile of those exposed to tropical

[1]Department of Medicine, Stanford University, Stanford, CA, USA. [2]Woods Institute for the Environment, Stanford University, Stanford, CA, USA. [3]Center on Food Security and the Environment, Stanford University, Stanford, CA, USA. [4]Department of Earth, Atmospheric, and Planetary Sciences, Purdue University, West Lafayette, IN, USA. [5]RAND Corporation, Santa Monica, CA, USA. [6]Institute of Health and Society, Université catholique de Louvain, Brussels, Belgium. [7]Johns Hopkins Center for Humanitarian Health, Department of International Health, Johns Hopkins University, Baltimore, MD, USA. [8]Department of Health Policy, Stanford University, Stanford, CA, USA. ✉e-mail: ebd@stanford.edu; zwagner@rand.org

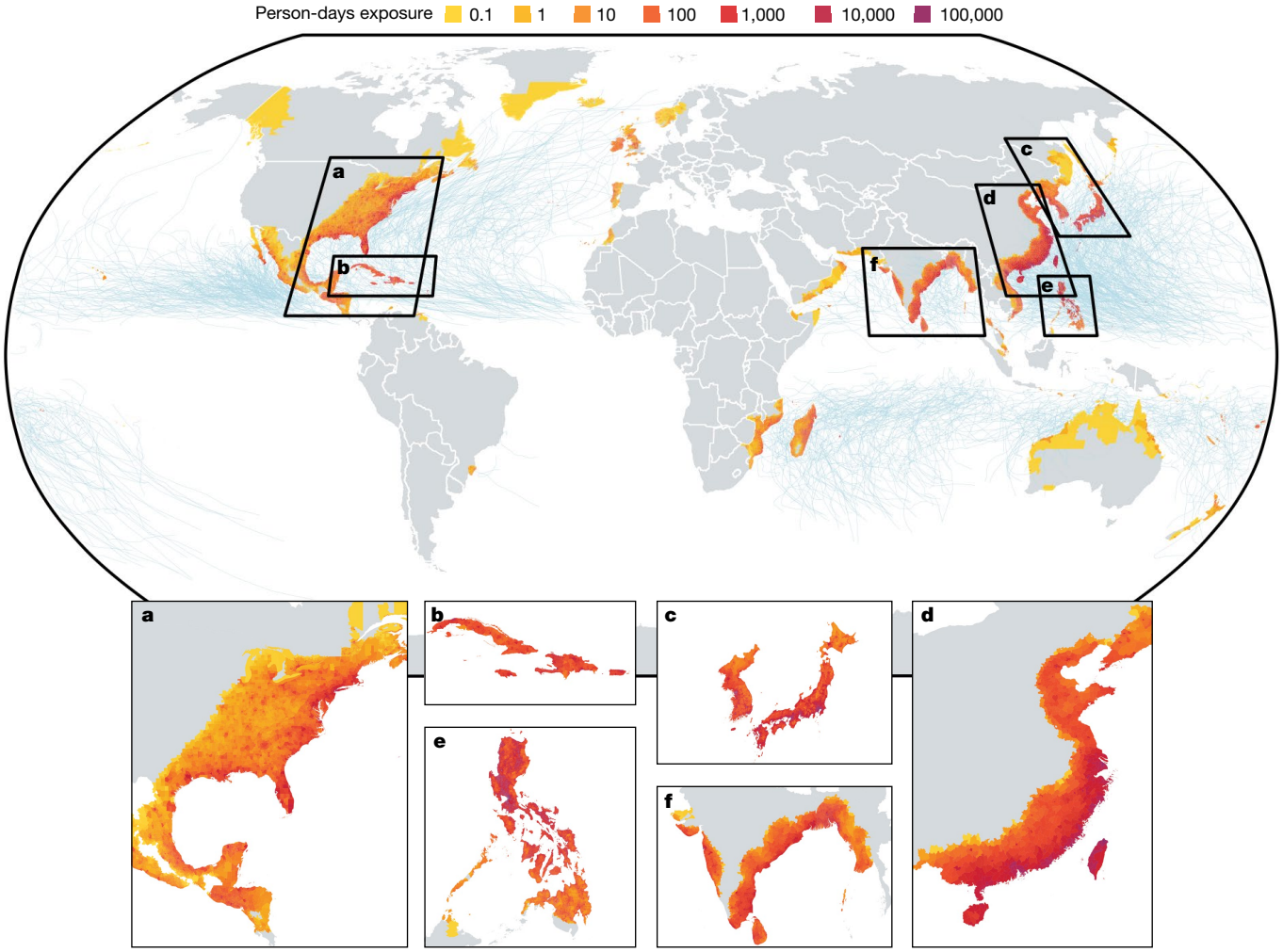

Fig. 1 | Global distribution of annual person-days exposure to tropical cyclones in 2002–2019. Storm tracks are shown by light-blue curves. **a**–**f**, Six sub-regions with high exposures are enlarged: Atlantic coastal North and Central America (**a**); the Caribbean (**b**); the Korean peninsula and Japan (**c**); coastal eastern Asia (**d**); South East Asia (**e**); and eastern India and Bay of Bengal (**f**). Countries/regions included in each subplot are listed in Extended Data Table 1. Country outlines were obtained from Global Administrative Areas, version 2.0 (http://www.gadm.org).

cyclones, including vulnerable groups such as children or older adults, and socioeconomic distribution, is important for understanding risk and for future planning. Here we provide evidence documenting the characteristics of the exposed populations and how this is evolving over time.

In this study, we characterize global population exposure to tropical cyclones from 2002 to 2019. We use a tropical cyclone parametric wind model that combines inner and outer storm dynamics[23] and use a new wind modelling approach to explicitly consider the asymmetry of storms over land[24]. We simulate wind fields for each tropical cyclone and then rasterize global wind fields at 30-arcsec spatial resolution (approximately 1×1 km^2). Then we overlay these wind fields on gridded age-specific and sex-specific population estimates (approximately 1×1 km^2)[25] and a measure of relative deprivation[26] to analyse the global distribution of population exposure over time, across ages and by relative vulnerability (see Methods for more details on wind modelling and exposure analysis). We also quantify the degree to which the patterns in tropical cyclone population exposure are driven by population growth versus changing tropical cyclone frequency and intensity. Our estimates of population exposure trends and the extent to which tropical cyclones affect vulnerable demographic groups are a foundation for assessing the global burden and future risks of tropical cyclones.

Global population exposure in 2002–2019

Tropical cyclones affected populations in 117 countries and regions between 2002 and 2019, with a few regions accounting for most of the exposure. We estimate that 95% of all person-days exposure (defined as the product of annual tropical cyclone days and population size; see Methods) during the study period come from Atlantic coastal North and Central America (5%), the Caribbean (3%), the Korean peninsula and Japan (6%), coastal eastern Asia (43%), South East Asia (24%) or eastern India and Bay of Bengal (14%) (see Fig. 1; countries/regions included are listed in Extended Data Table 1). The top five countries/regions with the highest person-days exposure are coastal China (33% of total person-days), Japan (19%), the Philippines (10%), Taiwan (9%) and the USA (4%), which collectively make up more than 75% of all exposed person-days. The next five countries/regions are all in Asia (see Supplementary Table 1).

For all storm intensities, we observe an increase in population exposure during the 18-year study period of 2002–2019 (see Fig. 2). We find similar patterns in person-days exposure (see Extended Data Fig. 2). We estimate that, during this period, approximately 560 million people on average were exposed to tropical cyclones with maximum wind speed of at least 63 km h^{-1} (that is, tropical storm or more intense) each year. Although our study period is not sufficiently long for inferences about

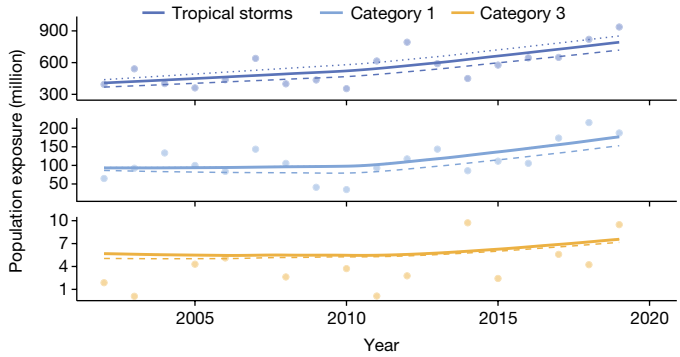

Fig. 2 | Global population exposure to tropical cyclones, 2002–2019. Top, middle and bottom curves represent exposure to tropical storms or larger (>63 km h^{-1} maximum wind speed), Category 1 or more intense (>119 km h^{-1} maximum wind speed) and Category 3 or more intense (>178 km h^{-1} maximum wind speed), respectively. Solid lines represent population exposure assuming up to 12 h of sustained wind over land, the dashed curves assume up to 6 h and the dotted lines assume no limit on duration of overland sustained wind. Point estimates represent raw data and curves represent the best fit of locally estimated scatterplot smoothing (LOESS). Population exposures to Category 3 winds in 2004 (15 million), 2007 (14 million), 2009 (<1,000), 2013 (10 million) and 2016 (11 million) are omitted for clarity but are included in the LOESS estimation. Most exposures occur within the first 12 h after landfall, especially for intense wind levels. For tropical storms, assuming 6 h and 12 h sustained wind over land are, on average, respectively 17% and 9% lower than assuming no limit of sustained winds over land. For Category 1 and Category 3 tropical cyclones, more than 90% population exposure occurred within the first 6 h after the storm made landfall, and almost all exposures occurred within 12 h after landfall.

long-term trends[27], we observe that population exposure increased from 408 million people in 2002 to 792 million people in 2019 using smooth estimates (raw estimates range from 354 million people in 2010 to 936 million people in 2019). The size of the estimated exposed population varied on the basis of storm intensity. Around 115 million people were exposed to tropical cyclones of at least Category 1 severity (maximum wind speed greater than 119 km h^{-1}; with a range of 35 million in 2010 and 215 million in 2018) per year and 5.8 million people on average were exposed to high-intensity tropical cyclones of at least Category 3 severity (>178 km h^{-1} maximum wind speeds; fewer than 1,000 in 2009 and 17 million people in 2004). These estimates do not represent unique individuals, as people exposed over several years would be counted for each respective year of exposure.

Age and sex profile

Certain groups, including young children and older populations, are thought to be particularly vulnerable to natural disasters[28,29]. To assess the extent to which vulnerable age groups are affected by tropical cyclones and how this is changing over time, we analyse the age composition of those exposed to the wind level of tropical storm or greater and compare annual exposure across two periods: 2002–2006 and 2015–2019. Figure 3 shows an overall shift in the age distribution of those exposed away from children (less than 5 years old) to older adults (more than 60 years old). On average, around 109.4 million older adults were exposed per year in 2015–2019 (95.0 million in Asia, 8.4 million in North America and 0.3 million in Africa) compared with 52.6 million per year in 2002–2006 (44.0 million in Asia, 5.9 million in North America and 0.34 million in Africa), a more than doubling of exposure. The number of children less than 5 years of age exposed to tropical cyclones increased from 57.3 million to 87.9 million per year, a 53% increase. In total, around 197 million children and elderly were exposed to tropical cyclones annually between 2015 and 2019. These shifts mirror the general population ageing patterns in Asia, North America and Europe[30].

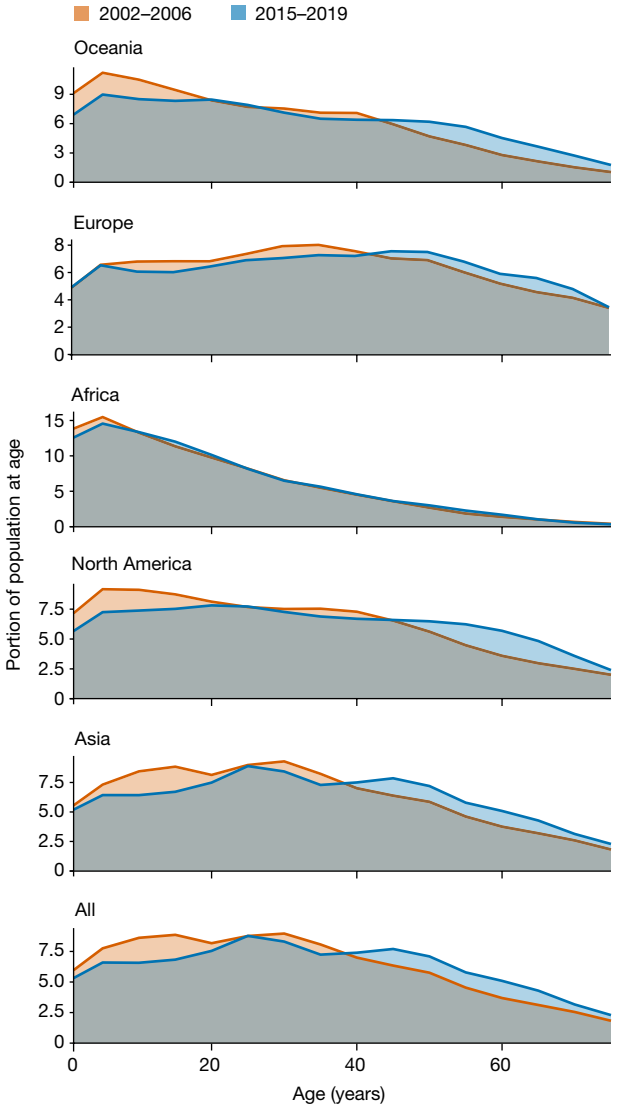

Fig. 3 | Age distribution of populations exposed to tropical cyclones. An overall shift in age distribution from young to old is observed globally when comparing the periods 2002–2006 and 2015–2019. The global shift mirrors the shifts in Asia and North America, which have the most people exposed. No notable changes were observed in Africa, probably because of the rapid growth of its young population. The *x* axes represent age groups with a 5-year interval from 0 to 75 years and the *y* axes represent the probability density function of age distributions. Globally, 57 million more older people (>60 years old) are exposed to tropical cyclones compared with the earlier study period.

The male-to-female ratio is similar between exposed and unexposed populations in all age groups and throughout the study period (results not shown).

Poverty and deprivation profile

Next we characterize the exposed population in terms of socioeconomic vulnerability as represented by the relative deprivation index[26] (RDI; details in Methods). We assess relative deprivation by calculating the RDI ratio as the quotient of the population-weighted RDI for the exposed population in a country and the population-weighted RDI for the unexposed population in the same country. An RDI ratio above 1 indicates that the exposed population is more deprived than the unexposed population. Figure 4 shows the result of this exercise for countries exposed to Category 1 or more intense storms between

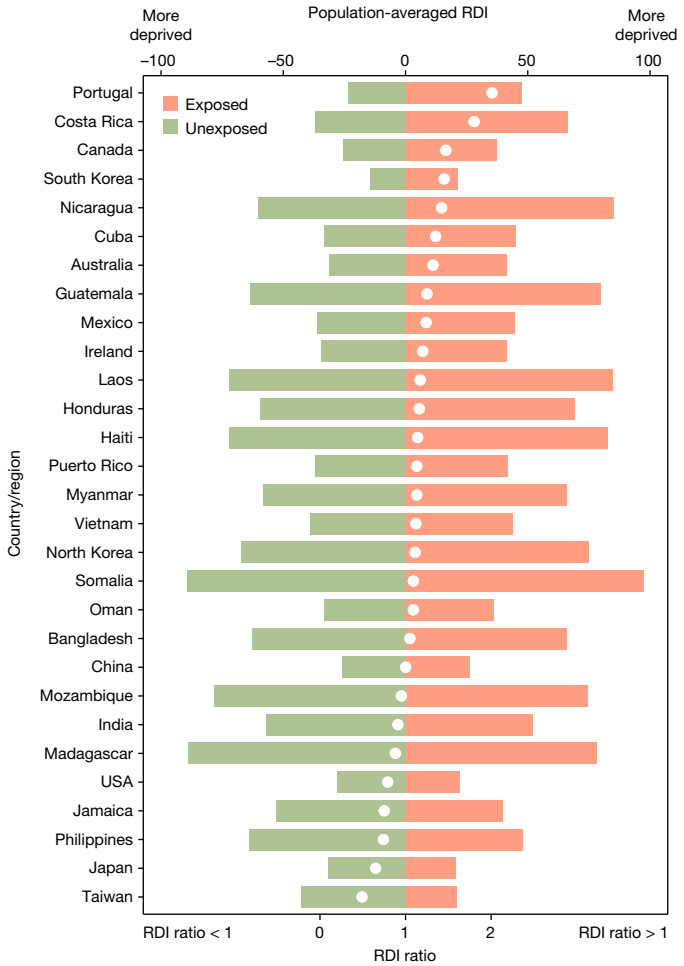

Fig. 4 | Population-weighted RDI ratio in each country/region. The population-weighted RDI for both exposed and unexposed populations (top axis, coloured bars), as well as the ratio of RDI between exposed and unexposed populations (bottom axis, white dots) in each country/region. The results are based on 29 countries/regions that have been exposed to Category 1 or more intense storms in 2010–2019. Countries/regions with a total population less than 100,000 or area smaller than 8,000 km^2 were omitted for clarity. Countries/regions are ordered in the RDI ratio rank in ascending order. Countries/regions above China (20/29) have RDI ratio greater than 1, for which exposed populations are more deprived than unexposed populations. Figure for all countries/regions without filtering by population or area is shown in Extended Data Fig. 7c.

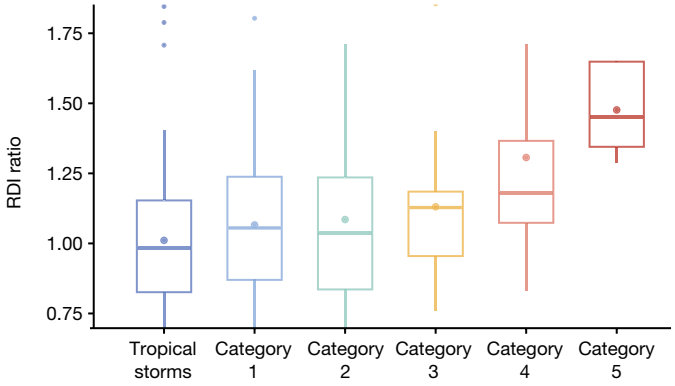

Fig. 5 | The relative deprivation is accentuated with increasing storm severity. Populations exposed to tropical cyclones are socioeconomically more deprived than unexposed populations and this trend is accentuated with increasing storm severity. In countries/regions exposed to Category 5 tropical cyclones, exposed populations have an average deprivation index 45% higher than unexposed populations. The upper, middle and lower boundaries of each box correspond to the 75th percentile, median and 25th percentile, respectively, of the RDI ratios among all countries affected by specific tropical cyclone wind intensities. The dots in each box represent the mean RDI ratio for the corresponding wind level. Dots outside the boxes represent outliers in each wind category. In total, 70, 48, 33, 20, 16 and 5 countries/regions with population size greater than 100,000 were exposed to tropical storms, Category 1, Category 2, Category 3, Category 4 and Category 5 wind speeds, respectively. The five countries/regions exposed to Category 5 or more intense storms are the Philippines, Mexico, the Bahamas, Fiji and Cuba.

2010 and 2019, organized by a decreasing RDI ratio. We find that, in 20 out of 29 countries/regions, exposed populations are relatively more deprived (RDI ratio > 1) and the average RDI ratio across all countries is 1.13. In other words, exposed populations, on average, have a 13% higher RDI than those unexposed in the same country.

This pattern is accentuated with increasing storm severity (see Fig. 5). Although the RDI of those exposed to the wind level of tropical storm is similar to those unexposed (median RDI ratio: 1.02; interquartile range: 0.91–1.18), the ratio increases with higher storm intensities. In countries exposed to Category 5 or more intense tropical cyclones, those exposed live in areas with RDI measures roughly 45% greater than those unexposed (median RDI ratio: 1.45; interquartile range: 1.35–1.65).

Role of population growth in tropical cyclone exposure

The growth in tropical cyclone population exposure over the study period reflects a combination of population growth and changes in tropical cyclone hazards. To decompose their relative contributions, we hold population size constant at 2002 levels and re-estimate exposure over time (see Extended Data Fig. 8). Holding population fixed, the smoothed change in population exposure from 2002 to 2019 is 33% lower than our base estimates that include population growth. This implies that one-third of the change in exposure is attributable to population growth, whereas the other two-thirds is because of changes in tropical cyclone hazards. A similar distribution is also observed for Category 1 tropical cyclones, in which changes in tropical cyclone climatology contribute 71% of the total increase. However, for Category 3 and larger storms, changes in tropical cyclone hazards contribute only 29% of the observed increase. The conclusions are similar when we use person-days exposure rather than population exposure (see Extended Data Fig. 8).

Sensitivity analyses

We assess the uncertainty in our primary findings in several ways. First, we use alternative wind modelling approaches (further details in Methods). Extended Data Fig. 3 shows the range of estimated population exposure using these different approaches. This figure shows that, although the levels vary by modelling approach, the trends are similar across modelling approaches. We also assess the sensitivity of the age distribution and relative deprivation to modelling approaches. These are shown in Extended Data Fig. 4 (for age distribution), Extended Data Fig. 6, Extended Data Fig. 7 and Extended Data Table 2 (for relative deprivation). Although some estimates change from one approach to another (for example, the country with the greatest RDI ratio changes based on the modelling approach), the overall patterns (of shifting age distribution from young to old and of greater relative deprivation among the exposed in most countries) are robust to how wind fields are modelled.

Finally, Fig. 2 also shows the range in exposure estimates based on assumptions about the duration of sustained winds over land. Our main modelling approach assumes that exposure stops 12 h after landfall, and we test sensitivity by assuming 6 h and unlimited sustained wind

duration. Figure 2 shows that most exposure occurs within the first 12 h after landfall (that is, assuming that unlimited sustained wind does not add much exposure), especially for more intense wind levels. Estimates of exposure to larger storms (such as Category 3 or more intense storms) are more sensitive to assumptions about sustained wind speed duration than that for weaker storms, which is consistent with the greater uncertainty in modelling the tropical cyclone inner core wind field[31].

Discussion and conclusions

In the first two decades of the twenty-first century, approximately 560 million people per year on average were exposed to tropical cyclones. This analysis provides a detailed profile of exposed populations and we identify five key findings: (1) the number of people exposed to tropical cyclones has increased between 2002 and 2019; (2) these increases hold for low-intensity and high-intensity cyclones, across different measures of exposure and nearly all affected world regions (Extended Data Fig. 1); (3) the age distribution of the exposed population has been shifting from young to old, mirroring demographic shifts in North America and Asia; (4) exposed populations are relatively more disadvantaged than unexposed populations; and (5) this relative disadvantage of the exposed population is more pronounced for more intense tropical cyclones.

Between 6% and 12% of the global population is exposed to tropical cyclones yearly. A large portion of exposure occurs at lower wind velocities. Although more intense storms, characterized by high wind velocities and precipitation, have received more attention from the research and policy communities, recurrent tropical storm and Category 1 storms are more common and extensive, with unknown human and economic burdens[32]. This more common exposure can have a disproportionate impact on low-income and middle-income countries, especially in regions in which resilience is limited and vulnerability is high.

We contextualize our exposure estimates relative to three sources. First, the Emergency Event Database estimates that about 24 million people per year were affected by tropical cyclones between 2001 and 2020 (ref. 11). These estimates are based on news sources, insurance claims and public reports. In that sense, it underscores the point that tropical cyclones receiving media attention are an underestimate of population exposure, especially for populations without reliable news or public reporting systems and which may not have material damages collected through insurance claims.

Second, Peduzzi et al.[22] estimate population exposure to tropical cyclones based on a decade-long average of tropical cyclone frequency and gridded total population estimates. During the period from 2002 to 2009, our estimates are, on average, 320% (4.2-fold) larger than Peduzzi et al.'s estimates for the decade 2000–2009. Third, Geiger et al.[7], using total population counts and an older tropical cyclone wind model with greater outer cyclone wind speeds, generate estimates that are, on average, 29% higher than ours. Our study uses wind modelling approaches that have been calibrated to account for storm asymmetry and terrain features after landfall, which improves the outer cyclone wind speed estimations (see Methods for an extensive discussion).

Over the study years considered, we observe an increase in overall population exposure across all wind intensity levels. However, there was substantial year-to-year variability in population exposure to the most intense storms, which is consistent with the findings of Wang and Toumi[33]. Increased exposure is attributed more to changes in tropical cyclone hazards than to population growth, and this is more pronounced for moderate-intensity storms. During the study period, the main characteristic of tropical cyclones that has changed is an increase in the intensity of the storm at landfall[33]. The rate of inland decay after landfall may also change, although this remains unclear[34–36]. Storm size has not changed substantially and is not expected to change with the warming climate[37,38]. In terms of population growth, the global population experienced not only a general increase of 22% but also a more substantial growth in urban and coastal populations[39], which has played a role in increased exposure. As noted, the time period of our study limits inferring about longer-term trends in tropical cyclone exposure. However, if the projections of the Intergovernmental Panel on Climate Change are correct, indicating an expected increase in the proportion of strong tropical cyclones in the future, along with an increase in the maximum wind speed of intense storms[2,40], it is reasonable to expect a continuing upward trend in population exposure to the most intense storms.

We document a shift in the age distribution of the exposed population, reflecting relatively fewer children and more elderly being exposed over time. Both young and old people are at increased risk of adverse consequences, including lack of access to essential healthcare, destruction of facilities and roads, power outages and insecure access to water and food[10,41,42]. Older populations, more than young, may also face mobility problems that hinder their ability to respond to disasters by evacuating landfall areas[16].

We also document that exposed populations are more socioeconomically deprived than unexposed populations, especially those exposed to high-intensity storms. One possible mechanism for this is selection: people with more means move away from regions at high risk of intense storms, leaving high-risk areas for those with lower socioeconomic status. Another mechanism is that storms, especially high-intensity storms, have a negative impact on socioeconomic development. The RDI ratio shows substantial heterogeneities, which could reflect resilience to natural disasters (greater resilience may reduce selection of residence based on exposure risk), exposure patterns (greater exposure may increase risk, but may also increase resilience) or the capacity for population adaptation. These mechanisms may operate to different extents and we are not able to disentangle these effects. Nevertheless, recognizing the relatively higher deprivation of those living in areas at risk for tropical cyclones may help give priority to adaptation and mitigation resources. This may be particularly salient in countries in which coastal regions at risk of tropical cyclones are more impoverished for other reasons, such as having few economic opportunities for seafaring occupations.

This study has several limitations. First, the population estimates provided by WorldPop are annual and do not reflect intra-annual population mobility. If individuals leave high-risk areas during the tropical cyclone season, resulting in a lower population count in exposed regions at the time of the event, then the annual average we use may overestimate actual population exposure. Although we cannot quantify the extent of this effect on our population exposure estimates, existing studies estimating short-term displacement (such as seasonal migration) indicate that only a minor portion of the population leave[43]. The fact that our population estimates do not capture seasonal migration could also have implications for the age and socioeconomic profiles we report. Those capable of moving away from the path of a tropical cyclone might be younger and of higher socioeconomic status than those not displaced, further accentuating the patterns we find for the age skew and socioeconomic deprivation of those actually exposed.

Second, tropical cyclone parametric wind models use simplifying assumptions based on storm structures over the ocean. When storms move over land, their structure is disrupted by land features, resulting in uneven wind decay. The field of tropical cyclone modelling is developing better representations of overland storm behaviour, but this remains an area of uncertainty. We demonstrate that all of our main results are robust to using several different modelling approaches.

Third, we represent socioeconomic vulnerability using a deprivation index, which reduces complexity to a single metric and does not include factors such as social marginalization, healthcare resources, critical infrastructures and governance, among others. Our deprivation index is not longitudinally available and does not capture population

displacement or socioeconomic development. We therefore present a cross-sectional view of the relationship of tropical cyclones to socioeconomic deprivation and are unable to examine temporal trends. As the work on granular variation in global socioeconomic conditions evolves, its relationship with tropical cyclones would be important future work.

In this study, we describe the composition of populations that have been exposed to tropical cyclones globally from 2002 to 2019. Using global gridded population and wind field data, we are able to capture exposure to intense storms and storms of lesser intensity. Our analysis indicates that population exposure to tropical cyclones increased from 408 million to 792 million people annually over the study period (560 million on average). The age composition in the exposed population has been transitioning from younger demographics to older ones, reflecting broader global demographic changes. We also find that populations exposed to tropical cyclones tend to be more disadvantaged compared with those not exposed, suggesting that these events can exacerbate existing inequalities and highlighting the need for targeted interventions to support vulnerable populations.

Online content

Any methods, additional references, Nature Portfolio reporting summaries, source data, extended data, supplementary information, acknowledgements, peer review information; details of author contributions and competing interests; and statements of data and code availability are available at https://doi.org/10.1038/s41586-023-06963-z.

1. Romanello, M. et al. The 2022 report of the *Lancet* Countdown on health and climate change: health at the mercy of fossil fuels. *Lancet* **400**, 1619–1654 (2022).
2. IPCC *Climate Change 2022: Impacts, Adaptation and Vulnerability* (eds Pörtner, H.-O. et al.) (Cambridge Univ. Press, 2022).
3. Kelman, I. Climate change and the Sendai Framework for Disaster Risk Reduction. *Int. J. Disaster Risk Sci.* **6**, 117–127 (2015).
4. Emanuel, K. Increasing destructiveness of tropical cyclones over the past 30 years. *Nature* **436**, 686–688 (2005).
5. *Sendai Framework for Disaster Risk Reduction 2015–2030* (United Nations Office for Disaster Risk Reduction, 2015).
6. *Spatial Hazard Events and Losses Database for the United States, Version 21.0* (Center for Emergency Management and Homeland Security, 2023).
7. Geiger, T., Frieler, K. & Bresch, D. A. A global historical data set of tropical cyclone exposure (TCE-DAT). *Earth Syst. Sci. Data* **10**, 185–194 (2018).
8. Geiger, T., Gütschow, J., Bresch, D. N., Emanuel, K. & Frieler, K. Double benefit of limiting global warming for tropical cyclone exposure. *Nat. Clim. Change* **11**, 861–866 (2021).
9. Deryugina, T. & Molitor, D. *Does When You Die Depend on Where You Live? Evidence from Hurricane Katrina* Working Paper 24822 (National Bureau of Economic Research, 2018).
10. Kishore, N. et al. Mortality in Puerto Rico after Hurricane Maria. *N. Engl. J. Med.* **379**, 162–170 (2018).
11. *2021 Disasters in Numbers* (Centre for Research on the Epidemiology of Disasters, 2022).
12. Emanuel, K. et al. Tropical cyclones. *Annu. Rev. Earth Planet. Sci.* **31**, 75–104 (2003).
13. Knutson, T. R. et al. Tropical cyclones and climate change. *Nat. Geosci.* **3**, 157–163 (2010).
14. Guha-Sapir, D. & Hoyois, P. *Estimating Populations Affected by Disasters: A Review of Methodological Issues and Research Gaps* (Centre for Research on the Epidemiology of Disasters, 2015).
15. Hsiang, S. M. & Jina, A. S. *The Causal Effect of Environmental Catastrophe on Long-Run Economic Growth: Evidence from 6,700 Cyclones* Working Paper 20352 (National Bureau of Economic Research, 2014).
16. Morita, T. et al. Excess mortality due to indirect health effects of the 2011 triple disaster in Fukushima, Japan: a retrospective observational study. *J. Epidemiol. Community Health* **71**, 974–980 (2017).
17. Islam, M. Q. et al. Children's vulnerability to natural disasters: evidence from natural experiments in Bangladesh. *World Dev. Perspect.* **19**, 100228 (2020).
18. Bhuiyan, T. R. et al. Disaster loss indicators for reporting to DesInventar Sendai and enabling rapid monetary valuation in Malaysia. *Weather Clim. Extrem.* **37**, 100488 (2022).
19. Mazhin, S. A. et al. Worldwide disaster loss and damage databases: a systematic review. *J. Educ. Health Promot.* **10**, 329 (2021).
20. Mavhura, E. & Aryal, K. R. Disaster mortalities and the Sendai Framework Target A: insights from Zimbabwe. *World Dev.* **165**, 106196 (2023).
21. Guha-Sapir, D., Below, R. & Hoyois, P. EM-DAT: International Disaster Database. *Catholic University of Louvain: Brussels, Belgium* **27**, 57–58 (2015).
22. Peduzzi, P. et al. Global trends in tropical cyclone risk. *Nat. Clim. Change* **2**, 289–294 (2012).
23. Chavas, D. R., Lin, N. & Emanuel, K. A model for the complete radial structure of the tropical cyclone wind field. Part I: comparison with observed structure. *J. Atmos. Sci.* **72**, 3647–3662 (2015).
24. Chen, J. et al. A new framework for evaluating model simulated inland tropical cyclone wind fields. *Geophys. Res. Lett.* **50**, e2023GL104587 (2023).
25. Tatem, A. J. WorldPop, open data for spatial demography. *Sci. Data* **4**, 170004 (2017).
26. *Global Gridded Relative Deprivation Index (GRDI), Version 1* (Center for International Earth Science Information Network, 2022); https://doi.org/10.7927/3xxe-ap97.
27. *WMO Guidelines on the Calculation of Climate Normals* (WMO, 2017).
28. Ngo, E. B. When disasters and age collide: reviewing vulnerability of the elderly. *Nat. Hazards Rev.* **2**, 80–89 (2001).
29. Peek, L. Children and disasters: understanding vulnerability, developing capacities, and promoting resilience – an introduction. *Child. Youth Environ.* **18**, 1–29 (2008).
30. *World Population Prospects 2022* (United Nations Department of Economic and Social Affairs, Population Division, 2022); https://population.un.org/wpp/Graphs/DemographicProfiles/Pyramid/900.
31. Yan, D. & Zhang, T. Research progress on tropical cyclone parametric wind field models and their application. *Reg. Stud. Mar. Sci.* **51**, 102207 (2022).
32. *Global Assessment Report on Disaster Risk Reduction 2019* (United Nations Office for Disaster Risk Reduction, 2019).
33. Wang, S. & Toumi, R. More tropical cyclones are striking coasts with major intensities at landfall. *Sci. Rep.* **12**, 5236 (2022).
34. Li, L. & Chakraborty, P. Slower decay of landfalling hurricanes in a warming world. *Nature* **587**, 230–234 (2020).
35. Chan, K. T., Zhang, K., Wu, Y. & Chan, J. C. Landfalling hurricane track modes and decay. *Nature* **606**, E7–E11 (2022).
36. Zhu, Y.-J., Collins, J. M. & Klotzbach, P. J. Spatial variations of North Atlantic landfalling tropical cyclone wind speed decay over the continental United States. *J. Appl. Meteorol. Climatol.* **60**, 749–762 (2021).
37. Knutson, T. R. et al. Global projections of intense tropical cyclone activity for the late twenty-first century from dynamical downscaling of CMIP5/RCP4.5 scenarios. *J. Clim.* **28**, 7203–7224 (2015).
38. Schenkel, B. A. et al. North Atlantic tropical cyclone outer size and structure remain unchanged by the late twenty-first century. *J. Clim.* **36**, 359–382 (2023).
39. Neumann, B., Vafeidis, A. T., Zimmermann, J. & Nicholls, R. J. Future coastal population growth and exposure to sea-level rise and coastal flooding-a global assessment. *PLoS One* **10**, e0118571 (2015).
40. IPCC *Climate Change 2023: Synthesis Report* (eds Core Writing Team, Lee, H. & Romero, J.) (IPCC, 2023).
41. Miranda, D. S. & Choonara, I. Hurricanes and child health: lessons from Cuba. *Arch. Dis. Child.* **96**, 328–329 (2011).
42. Carroll, A. E. & Frakt, A. B. Children's health must remain a focus in the recovery from Hurricane Harvey. *JAMA Pediatr.* **171**, 1029–1030 (2017).
43. Wesolowski, A. et al. Multinational patterns of seasonal asymmetry in human movement influence infectious disease dynamics. *Nat. Commun.* **8**, 2069 (2017).

Methods

Tropical cyclone data from IBTrACS

Tropical cyclone tracks data used in this study are taken from the International Best Track Archive for Climate Stewardship (IBTrACS version v04r00)[44,45]. This database includes 6-hourly latitude and longitude tropical cyclone positions and maximum 1-min sustained wind of storm centre at 10 m above the sea surface. We use global tropical cyclone data between 2002 and 2019. We chose the start year to align with availability of data on storm extent in IBTrACS and the end year to align with gridded population estimates. Storm observations with a missing maximum wind speed or whose maximum wind speed is less than 34 knots (below the tropical storm threshold) are removed. Our storm dataset thus includes 1,808 tropical cyclone events in six global basins (North Atlantic, Western Pacific, Eastern Pacific, South Pacific, North Indian, South Indian).

Primary tropical cyclone wind modelling approach

To estimate the extent of wind exposure associated with tropical cyclones, we use a parametric model to estimate the complete wind field of each storm. In general, parametric wind models generate complete wind speed profiles with few inputs, making them suitable for global analyses such as ours. Although parametric models were originally calibrated using mature storms over the ocean, recent models account for the evolution of storms during landfall, and validation with observational data indicates good overland performance[24,46].

In this work, we use an approach developed by Chen et al.[24], based on the model introduced by Chavas et al. (referred to as 'C15')[23,47]. The C15 wind field model mathematically merges an inner wind field model (equation (36) in ref. 48) and a separate outer wind field (equations (31)–(33) in ref. 49), producing a complete azimuthal wind profile. The parameters required by C15 are: storm maximum wind velocity V_m, radius of maximum wind speed R_{max} for the inner region, radius of a specific intensity R_{fit} (for example, radius of 34-knot wind, R_{34}), Coriolis parameter f, exchange coefficients of momentum C_d and free tropospheric subsidence rate w_{cool}.

The approach we use is based on Chen et al.[24], which explicitly considers the asymmetry of storm structure after landfall. It applies the C15 model to each earth-relative quadrant, using quadrant-specific storm and surface parameters as model inputs. We refer to this approach as 'Quad-by-Quad'. This approach has been validated with an observational dataset of post-landfall storm wind speeds.

In C15, V_m and the storm latitude ϕ are taken from IBTrACS. The Coriolis parameter f is computed as a function of storm latitude. The radius of 34-knot wind R_{34} in each quadrant (northeast, northwest, southwest, southeast) are also taken from IBTrACS. The most specific parameter that accounts for the characteristics of the terrain, C_d, is calculated using surface roughness data[50] from ECMWF Reanalysis v5 (ERA5)[51]. It is averaged over a range of 0–600 km to yield a single value within each quadrant. Previous studies have shown that the wind field solution is not sensitive to the selection of w_{cool}. We set w_{cool} to be 0.002 m s^{-1}, which is consistent with the median of the best-fit value observed in storms[23] and identical to the value used elsewhere[46]. We use C15 and Quad-by-Quad jointly to simulate wind profiles in each quadrant and obtain complete tropical cyclone wind profiles.

In this approach, R_{fit} can use outer radii of any wind speed, such as R_{50} (radius of 50-knot wind). We use R_{34} as it has a non-zero value for all storms in this study, it can be accurately estimated by remote-sensing systems with little rain contamination and, in more recent years, it has undergone quality control in retrospective best track reanalysis[52]. In IBTrACS, R_{34} is available since 2002 and also reviewed post-season, or 'best tracked', since 2004 in the Atlantic/East Pacific and since 2015 in other global basins. Thus there is less uncertainty in our wind fields during the later years of the study period.

On the basis of this approach, we simulate tropical cyclone wind fields at 6-h intervals for each storm. Using that information, we calculate the annual maximum wind speed for each location and rasterize it at a 30-arcsec resolution. We then categorize the intensity of the storm in each affected area based on the annual maximum gridded wind speed.

Other wind modelling approaches for sensitivity tests

There is meaningful variation in wind modelling approaches. We model and run all analyses using two other approaches that enable global exposure estimates. The first approach is a modification of our primary Quad-by-Quad approach that takes into account possible overestimation in the outer reach of the storm. Following Chavas and Knaff[53], we reduce the outer radius R_{34} in each quadrant by a factor of 0.85. Because the outer radius R_{34} in IBTrACS is operationally defined as the outermost value within each quadrant, this might lead to an overestimation of the outer reach of the storm, and this reduction has been shown to have advantages in some contexts. This approach is referred to as 'Quad-by-Quad-0.85'.

Our second approach is based on C15 and we use a separate component to estimate the asymmetrical surface winds of tropical cyclones over land. In this approach, the total wind is estimated as the sum of two components: one is the axisymmetric component associated with the storm itself (modelled by C15) and the other is the asymmetric component caused by the combined effects of storm movement and ambient wind shear[54]. We label this approach as 'C15+LC12' in the figures. In this approach, the axisymmetric component simulated by C15 uses the radius of maximum wind speed R_{max} of a storm as model input. R_{max} plays a crucial role in representing the size of the inner region of the storm, which markedly affects the simulation of the intense wind region of the storm. Because R_{max} is estimated with more uncertainty than the outer size of the storm, we derive R_{max} from R_{34}, following Chavas and Knaff[53]. Specifically, we calculate R_{34} as the mean of all non-zero values available in each quadrant, multiplied by a factor of 0.85. Then we predict R_{max} based on R_{34} to get the radius of maximum wind speed. We use this approach to quantify the uncertainties in the strong-wind region of the storms, in which the Quad-by-Quad approach is incompletely validated[24].

WorldPop

We obtain estimates of human population distributions from WorldPop[25]. We extract spatial distributions of total population counts using WorldPop global mosaic files and age-specific population distributions using WorldPop age and sex structure files. WorldPop estimates population counts at a resolution of 30 arcsec degree (about 1 km) between 2000 and 2019. We merge population estimates with wind field estimates at the grid cell level.

We choose WorldPop as our primary source for gridded population estimates as it provides age-structured and sex-structured time series for population estimates between 2000 and 2019, at a sufficient resolution to match the constructed wind field estimates[55].

Tropical cyclone exposure

Using gridded tropical cyclone wind fields and population estimates, we estimate tropical cyclone exposures using two metrics. The first metric is an annual population exposure count, in which a population grid cell is counted as exposed if the maximum sustained wind exceeds a certain wind threshold at least once in the year:

$$\text{exposure}_{\text{year,grid}} = \max_{\text{day}\in\text{year}} \mathbb{1}(V_{\text{day,grid}}) = \begin{cases} 1, & \text{if } V_{\text{day,grid}} > V_{\text{thres}} \\ 0, & \text{if } V_{\text{day,grid}} \le V_{\text{thres}} \end{cases} \quad (1)$$

In equation (1), the subscript 'grid' represents each 30-arcsec-degree cell, $V_{\text{day,grid}}$ represents simulated maximum sustained wind speed for a specific cell on a given day and V_{thres} represents a specific wind speed threshold. On the basis of the affected grids identified in equation (1), the total population exposure in a given year is calculated as:

$$\text{annual population exposure}_{\text{year}} = \sum_{\text{grid}} \text{population}_{\text{year,grid}} \times \text{exposure}_{\text{year,grid}} \quad (2)$$

The second metric is annual person-days exposure, defined as the product of annual frequency under a specific wind speed threshold and the population size for each grid cell. Similarly, the annual days exposed to tropical cyclones for each grid is computed as follows:

$$\begin{aligned}\text{tropical cyclone days}_{\text{year,grid}} &= \sum_{\text{day}\in\text{year}} \mathbb{1}(V_{\text{day,grid}}) \\ &= \begin{cases} 1, & \text{if } V_{\text{day,grid}} > V_{\text{thres}} \\ 0, & \text{if } V_{\text{day,grid}} \le V_{\text{thres}} \end{cases}\end{aligned} \quad (3)$$

The total person-days exposure in a given year is computed as:

$$\text{annual person - days exposure}_{\text{year}} = \sum_{\text{grid}} \text{population}_{\text{year,grid}} \times \text{tropical cyclone days}_{\text{year,grid}} \quad (4)$$

We choose thresholds for maximum sustained wind speed based on categories on the Saffir–Simpson scale[56]. We use TS, CAT1, CAT2, CAT3, CAT4 and CAT5 to denote storm winds at tropical storm (34–63 knots), Category 1 (64–82 knots), Category 2 (83–95 knots), Category 3 (96–112 knots), Category 4 (113–136 knots) and Category 5 (≥137 knots) scales, respectively.

For all three parametric wind modelling approaches, we further quantify the uncertainties in the range of population exposure by assuming sustained wind up to 6 h (one step in IBTrACS data), 12 h (two steps) and no limit (full tracks) of duration over land. When storms stay longer over land after landfall, the uncertainty in R_{34} data increases and the structure of the storm becomes more asymmetric, which together lead to larger uncertainty in the estimates. That is, the population exposure estimates within 12 h after landfall are more reliable than the full tracks, and we use that duration in all our primary analyses.

Global gridded RDI

We use the global gridded RDI to represent the socioeconomic status of exposed and unexposed populations[26]. The RDI has a value between 0 and 100, for which higher values represent higher levels of deprivation. The RDI is constructed using six main sociodemographic components: gridded child dependency ratio, infant mortality rate at the various administrative levels, human development index (derived from life expectancy, mean years of schooling and gross national income) at the first administrative level, gridded building footprint, gridded nighttime lights and recent local deprivation trends. These six main components are harmonized and rasterized and the resulting RDI data have a resolution of 30 arcsec degree (about 1 km), with global coverage. The high spatial resolution of the RDI allows for capturing variations in socioeconomic profiles across different areas within the same country (see Extended Data Fig. 5).

To assess the socioeconomic profile of exposed populations, we define the RDI ratio as the quotient of the population-weighted RDI for the exposed population in a country and the population-weighted RDI for the unexposed population in the same country. Therefore, an RDI ratio exceeding 1 indicates that the exposed population is more deprived than the unexposed population.

The RDI is noted to be representative of the world in 2015. The raw data used to develop the RDI are either single-year or estimates between 2010 and 2020. We consider the RDI, then, as a single representation of the global levels of relative deprivation during the decade from 2010 to 2019. For all population exposure analyses using the RDI, we limit our sample to 2010–2019 to align with the RDI time frame.

Data availability

Replication data and codes for this study have been deposited at https://doi.org/10.5061/dryad.76hdr7t30.

44. Knapp, K. R., Diamond, H. J., Kossin, J. P., Kruk, M. C. & Schreck, C. J. *International Best Track Archive for Climate Stewardship (IBTrACS) Project, Version 4. v04r00* (NOAA National Centers for Environmental Information, 2018).
45. Knapp, K. R., Kruk, M. C., Levinson, D. H., Diamond, H. J. & Neumann, C. J. The International Best Track Archive for Climate Stewardship (IBTrACS): unifying tropical cyclone data. *Bull. Am. Meteorol. Soc.* **91**, 363–376 (2010).
46. Chen, J. & Chavas, D. R. A model for the tropical cyclone wind field response to idealized landfall. *J. Atmos. Sci.* **80**, 1163–1176 (2023).
47. Chavas, D. R. & Lin, N. A model for the complete radial structure of the tropical cyclone wind field. Part II: wind field variability. *J. Atmos. Sci.* **73**, 3093–3113 (2016).
48. Emanuel, K. & Rotunno, R. Self-stratification of tropical cyclone outflow. Part I: implications for storm structure. *J. Atmos. Sci.* **68**, 2236–2249 (2011).
49. Emanuel, K. in *Atmospheric Turbulence and Mesoscale Meteorology* (eds Fedorovich, E. et al.) 165–192 (Cambridge Univ. Press, 2004).
50. Hersbach, H. Sea surface roughness and drag coefficient as functions of neutral wind speed. *J. Phys. Oceanogr.* **41**, 247–251 (2011).
51. Hersbach, H. et al. The ERA5 global reanalysis. *Q. J. R. Meteorol. Soc.* **146**, 1999–2049 (2020).
52. Francis, A. S. & Strahl, B. R. *Annual Tropical Cyclone Report 2020* (Joint Typhoon Warning Center, 2021); https://www.metoc.navy.mil/jtwc/products/atcr/2020atcr.pdf.
53. Chavas, D. R. & Knaff, J. A. A simple model for predicting the tropical cyclone radius of maximum wind from outer size. *Weather Forecast.* **37**, 563–579 (2022).
54. Lin, N. & Chavas, D. On hurricane parametric wind and applications in storm surge modeling. *J. Geophys. Res. Atmos.* **117**, D09120 (2012).
55. Leyk, S. et al. The spatial allocation of population: a review of large-scale gridded population data products and their fitness for use. *Earth Syst. Sci. Data* **11**, 1385–1409 (2019).
56. Williams, J. Hurricane scale invented to communicate storm danger. *USA Today* (17 May 2007).
57. Holland, G. A revised hurricane pressure–wind model. *Mon. Weather Rev.* **136**, 3432–3445 (2008).

Acknowledgements E.B., R.J., S.H.-N., A.C.-G., D.G.-S., Z. Wang and Z. Wagner disclose support for the research and publication of this work from the NIH grant R01HD104835.

Author contributions E.B., Z. Wagner and R.J. conceived the idea. R.J. generated tropical cyclone wind data. M.G. processed population data. R.J. designed the study, performed the analysis and interpreted the results. R.J., S.H.-N., D.R.C., M.G., Z. Wang, A.C.-G., D.G.-S., E.B. and Z. Wagner drafted and revised the manuscript.

Competing interests The authors declare no competing interests.

Additional information

Supplementary information The online version contains supplementary material available at https://doi.org/10.1038/s41586-023-06963-z.

Correspondence and requests for materials should be addressed to Eran Bendavid or Zachary Wagner.

Peer review information *Nature* thanks Ralf Toumi and the other, anonymous, reviewer(s) for their contribution to the peer review of this work. Peer reviewer reports are available.

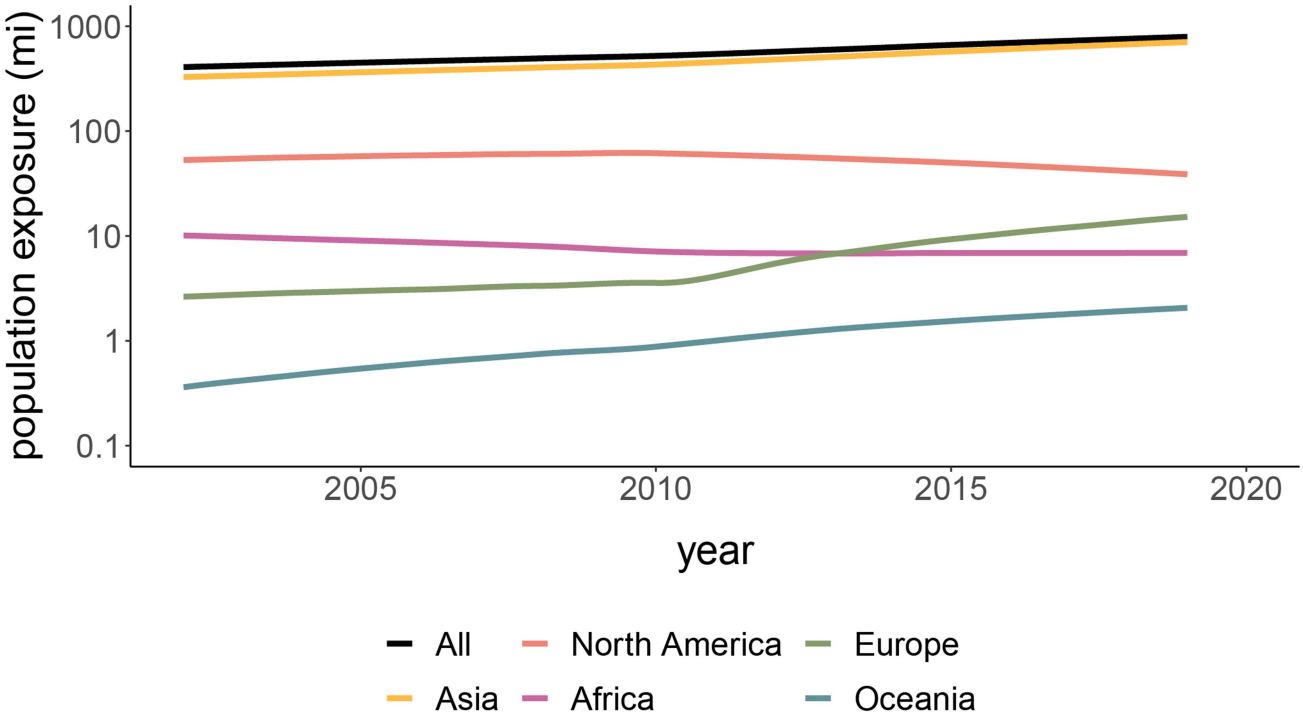

Extended Data Fig. 1 | Population exposure to tropical cyclones in 2002–2019, by continent. Curves represent exposure to tropical storms or higher winds (>63 km h^{-1} maximum wind speed), assuming 12-h duration of sustained wind over land. The overall increase in global exposure to tropical cyclones is primarily driven by Asia.

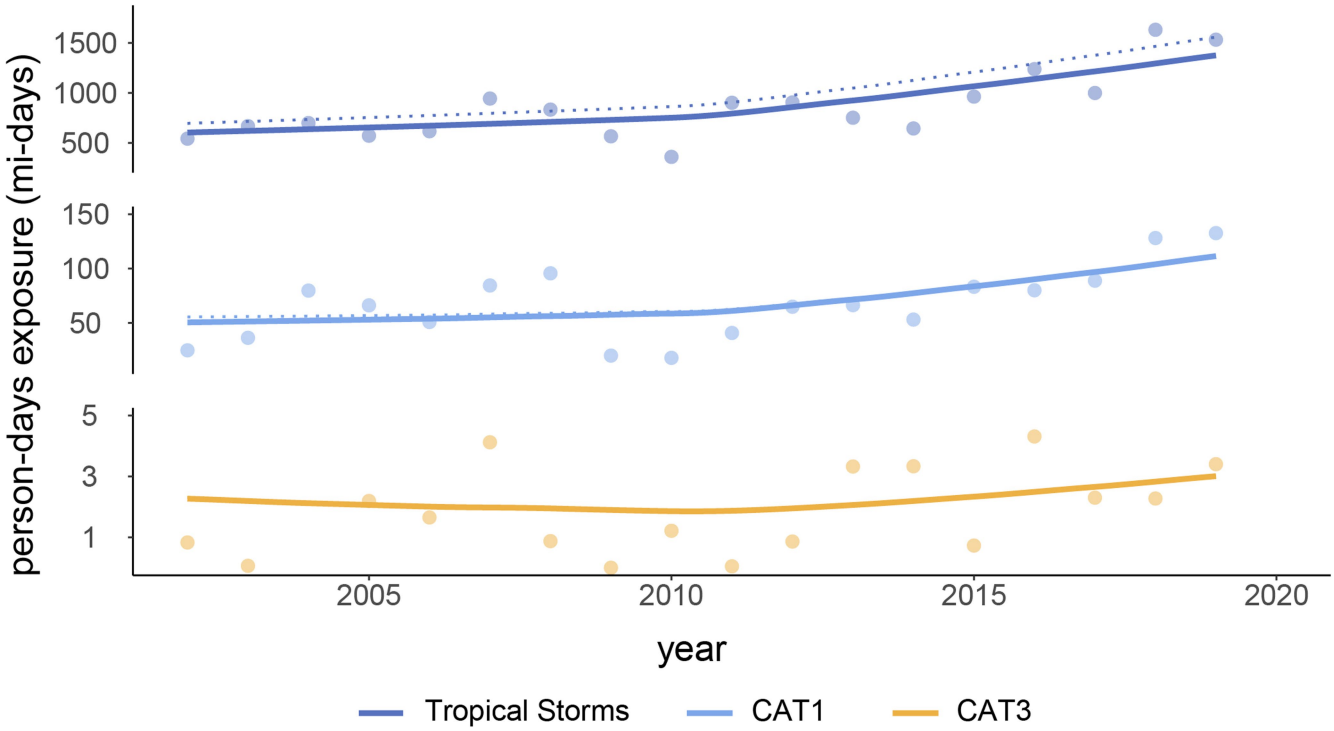

Extended Data Fig. 2 | Global person-days exposure to tropical cyclones in 2002–2019. Similar to Fig. 2, the person-days exposure has increased between 2002 and 2019. The top, middle and bottom curves represent person-days exposure to tropical storms, Category 1 or more intense and Category 3 or more intense storms, respectively. The solid, dashed and dotted lines represent exposure assuming up to 12 h, 6 h and no limit on duration of sustained wind over land. Point estimates represent raw data and the curves represent locally estimated scatterplot smoothing (LOESS) best fit. Increasing trends in person-days exposure are observed for all wind levels.

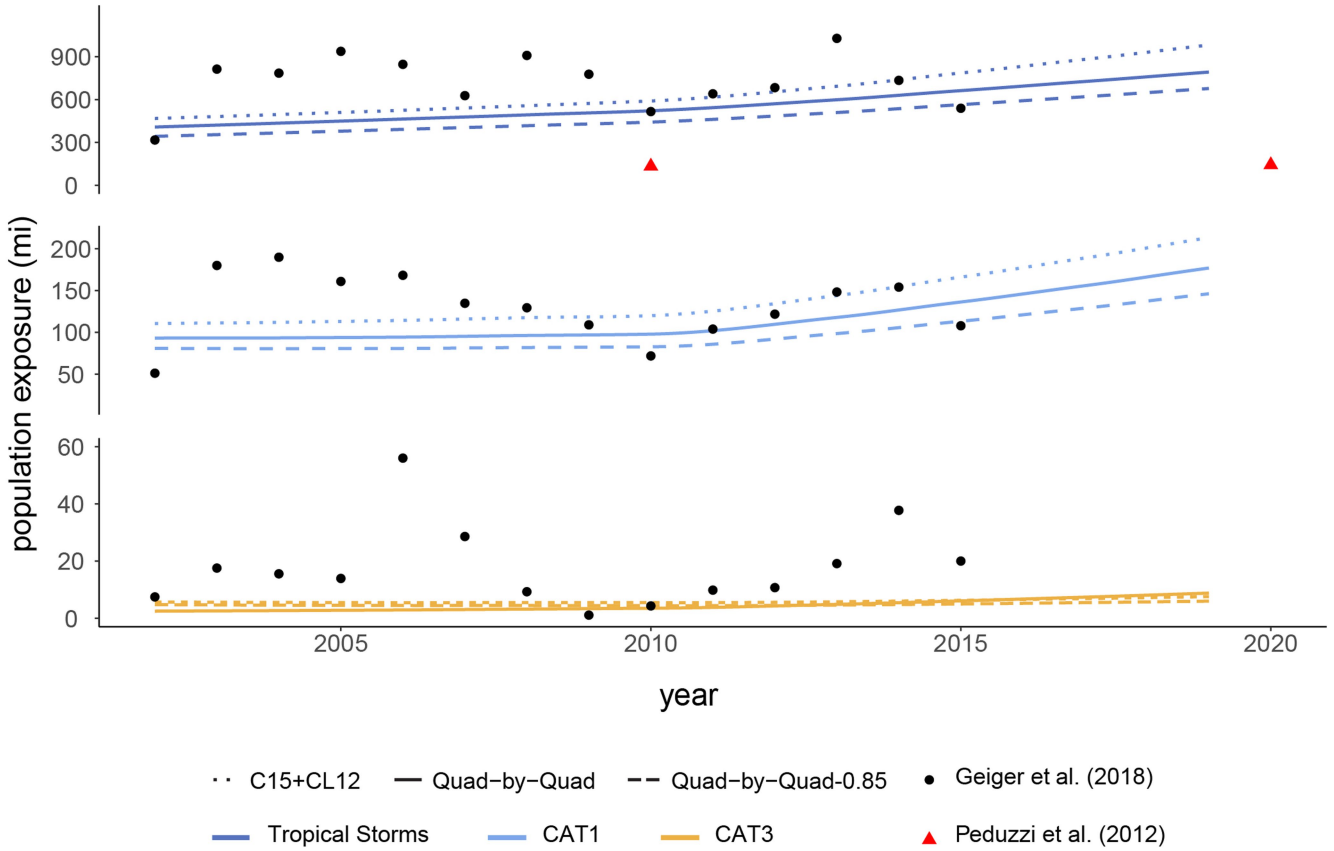

Extended Data Fig. 3 | Comparison of population exposure levels with different wind modelling approaches. The figure compares the population exposure estimates calculated using three different wind modelling approaches (the primary approach Quad-by-Quad with two other approaches, Quad-by-Quad-85 and C15+LC12). Similarly to the solid curves in Fig. 2, the coloured curves represent exposures to tropical storms or higher winds (>63 km h^{-1} maximum wind speed), assuming a 12-h duration of sustained wind over land. The estimates are further compared with population exposure estimates in previous studies, that is, Geiger et al.[7] and Peduzzi et al.[22]. Peduzzi et al. estimate population exposure based on a decade-long average, with the two red triangles representing estimates for the two decades of 2000–2020. This comparison indicates that: (1) the increasing trend from 2002 to 2019 is robust to model choice, and we observe this pattern with all three modelling approaches; (2) by correcting the outer radius through a reduction factor of 0.85, the population exposure reduces by approximately 15%, indicating that the impact of the reduction factor on estimated population exposure is approximately linear; (3) the uncertainty in population exposure to stronger storms is greater than that to weaker storms, and the disparities in the estimates of exposure to Category 3 or more intense storms can be as much as threefold in certain years; (4) despite the uncertainties in the exposure estimates obtained from the three different approaches, the difference is very small compared with previous studies. The discrepancy between our estimates and Geiger et al.[7] can be partially attributed to differences in the wind parametric method. Geiger et al. used a parametric wind model from Holland[57], which may potentially overestimate tropical cyclone surface winds.

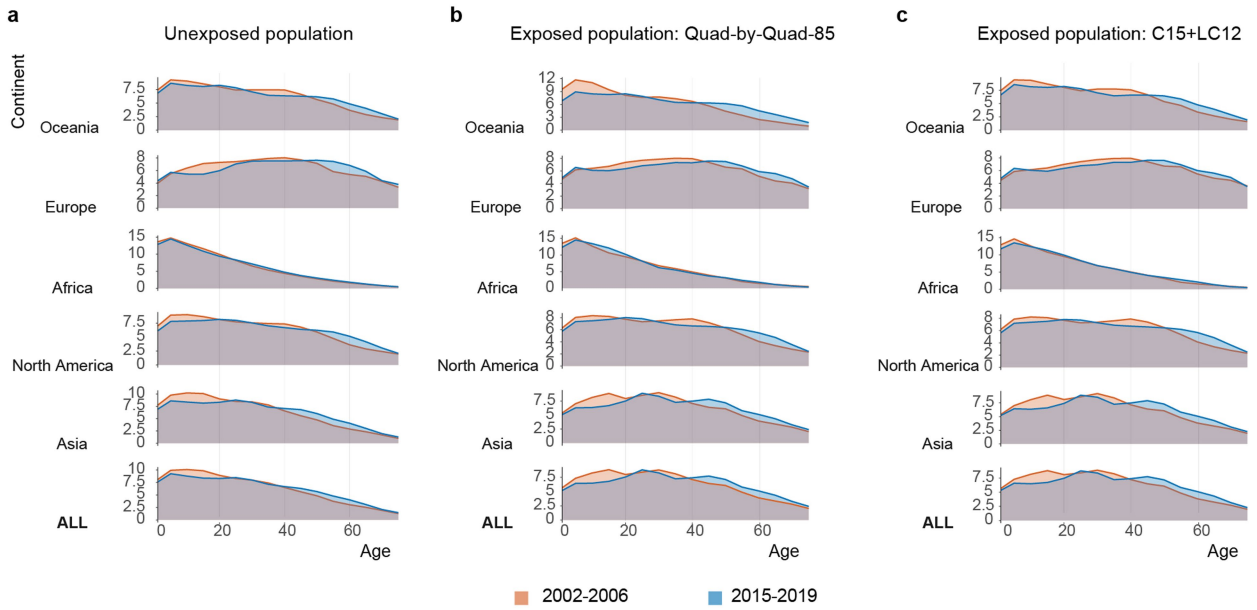

Extended Data Fig. 4 | Sensitivity analysis for age profile, as in Fig. 3. a, Age profile of unexposed population, indicating that the overall shift in the age distribution of exposed population is largely driven by the general population ageing patterns in Asia, North America and Europe. **b**,**c**, Age profiles for the exposed population identified by Quad-by-Quad-85 (**b**) and C15+LC12 (**c**), suggesting that the overall change in the age distribution of the exposed population is robust to model choice.

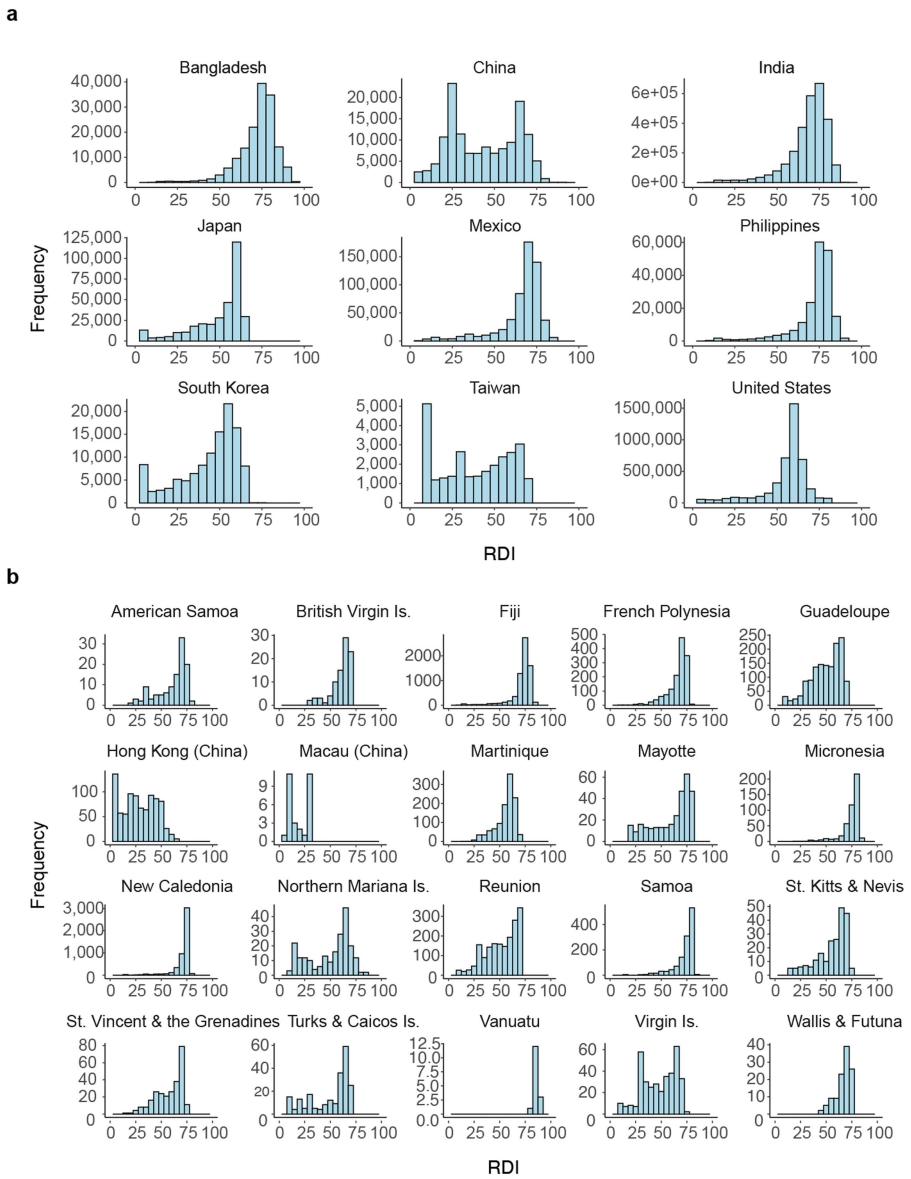

Extended Data Fig. 5 | Variations in the RDI of exposed countries/regions. The RDI is suitable for this analysis as it captures the variations in the socioeconomic profiles across different regions within the same country. Here we show the RDI distribution for the most heavily exposed nine countries/regions in **a** as an example. In Fig. 4, we exclude countries/regions with populations less than 100,000 or areas smaller than 8,000 km^2 for clarity. There are two reasons for removing these areas: first, in regions with small areas or low populations, everyone is affected by tropical cyclones, making the RDI ratio meaningless; second, in regions with small areas, there is insufficient variation in the RDI. In the two aforementioned circumstances, the RDI is not a suitable indicator, as we show in **b**. With this criterion, countries/regions removed in the RDI analyses are: Turks and Caicos Is., St. Kitts and Nevis, Virgin Is., Samoa, Vanuatu, St. Vincent and the Grenadines, Guadeloupe, British Virgin Is., Martinique, Micronesia, Mayotte, Wallis and Futuna, Reunion, American Samoa (Eastern Samoa), French Polynesia, Fiji, Macau (China), Hong Kong (China), New Caledonia and Northern Mariana Is. We show the RDI ratio of these countries/regions in Extended Data Fig. 6. In Fig. 5, we only exclude countries/regions with populations less than 100,000, so that the most intense wind category (Category 5) still has five countries/regions remaining. In Extended Data Fig. 7, we also confirm that the primary findings on the socioeconomic characteristics of the exposed population in this study remain valid, regardless of whether the countries/regions are included or excluded.

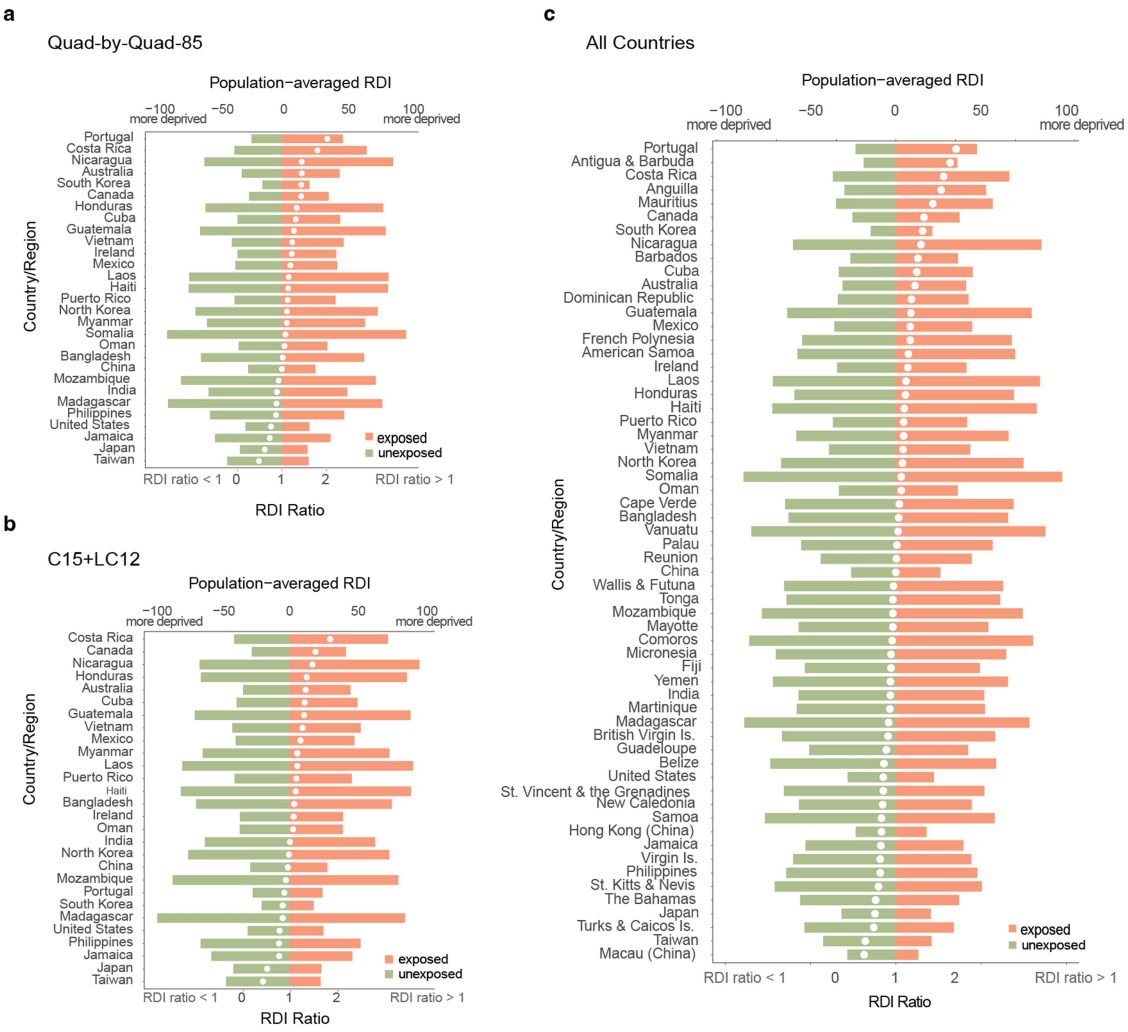

Extended Data Fig. 6 | Sensitivity analysis for the RDI ratio of exposed countries/regions, as in Fig. 4. Subplots **a** and **b** indicate that the main conclusion about the RDI ratio of exposed countries/regions is not sensitive to model choice. Here we present the RDI ratios of each affected country/region, identified by the Quad-by-Quad-85 modelling approach (**a**) and the C15+LC12 modelling approach (**b**). The raw results are listed in Extended Data Table 2. Our results show that 70% and 73% of the countries/regions have RDI ratios greater than 1, respectively. It is important to note that the RDI ratio for Portugal experiences substantial fluctuations when different wind modelling approaches are used. This is primarily because of the location of Portugal in a higher-latitude region, in which tropical cyclones have already undergone extratropical transition, which greatly affected the symmetric structure of the storm. In this scenario, the C15+LC12 approach is less suitable, and only the Quad-by-Quad method can capture this substantial asymmetry. When comparing the Quad-by-Quad-85 and Quad-by-Quad methods, the change in the RDI ratio for Portugal is minimal. **c**, The RDI ratio for all countries/regions exposed to Category 1 or more intense storms, including those with population less than 100,000 or area smaller than 8,000 km^2.

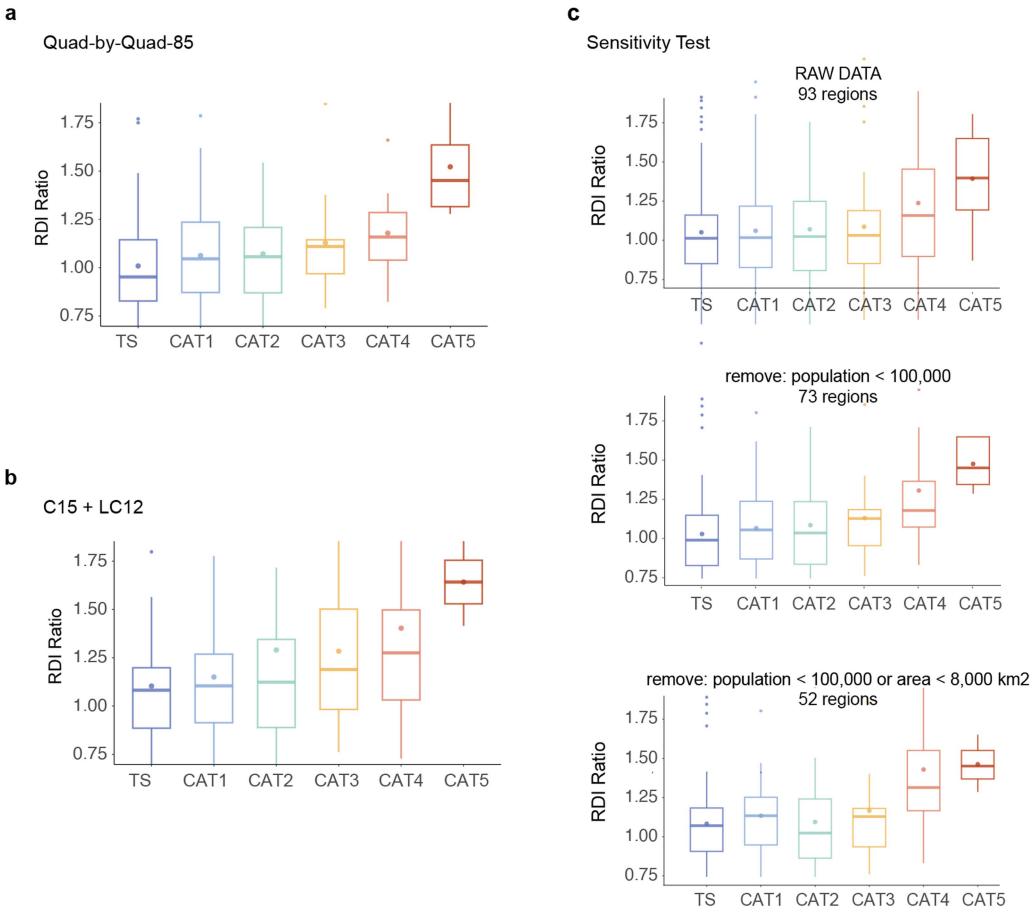

Extended Data Fig. 7 | Sensitivity analysis for the trends in the RDI ratio with increasing storm severity, as in Fig. 5. Subplots **a** and **b** indicate that the main conclusion about the socioeconomic profiles of the exposed population is not sensitive to model choice. Here we show results of the analysis similar to those shown in Fig. 5, but with exposed population identified with the Quad-by-Quad-85 modelling approach (**a**) and the C15+LC12 modelling approach (**b**). They both show similar patterns and the conclusion is robust. **c**, Sensitivity test based on our primary modelling approach Quad-by-Quad but using three different countries/regions subsets. The top plot includes the raw 93 countries/regions that were exposed to tropical cyclones between 2010 and 2019, the middle plot removes areas with populations less than 100,000 and the bottom plot removes countries/regions with populations less than 100,000 or areas smaller than 8,000 km^2. In all three subplots, we show that the exposed populations are more socioeconomically deprived than unexposed populations within the same country, and this relationship is more pronounced for higher-intensity storms. Our results indicate that this conclusion is robust and unaffected by the removal of small countries/regions.

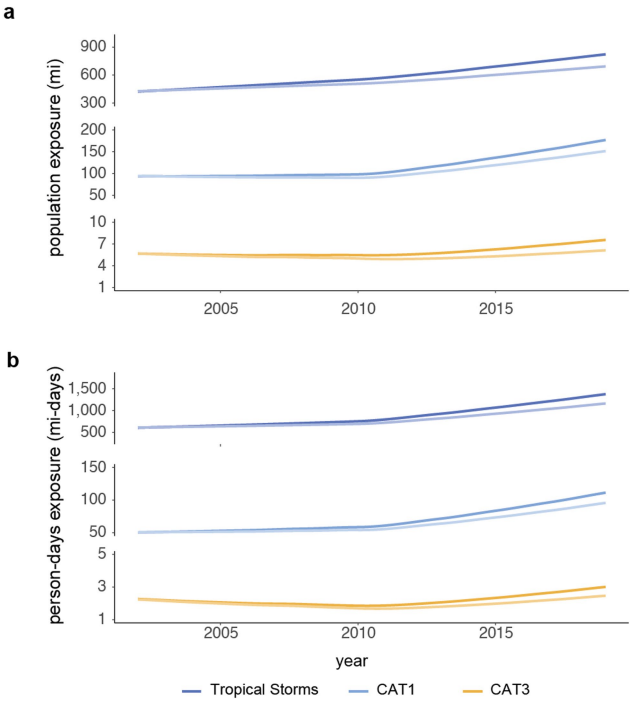

Extended Data Fig. 8 | Relative contributions of population growth and changes in tropical cyclone climatology to the change in tropical cyclone exposure. For each tropical cyclone wind intensity, we hold population size constant at the 2002 level and re-estimate population exposure over time, as shown by the light-coloured curve in each panel. We do this exercise for both population exposure (**a**) and person-days exposure (**b**). We show that around 67%, 71% and 29% of the change in total population exposure is attributable to the changes in tropical cyclone climatology at the tropical storms, Category 1 and Category 3 wind levels, respectively. Similarly, 72%, 74% and 27% of the change in person-days exposure is attributable to changes in tropical cyclone climatology at the tropical storms, Category 1 and Category 3 wind levels, respectively. The reasons behind the differences in the distribution between weak and intense storms remain uncertain and require further study.

Extended Data Table 1 | List of countries/regions in six most heavily exposed sub-regions shown in Fig. 1

Subplot	Sub-Regions	Countries/Regions
A	North and Central America	Canada, United States; Bermuda; Mexico; Guatemala; Belize; Honduras; El Salvador; Costa Rica
B	Caribbeans	Anguilla; Aruba; Barbados; British Virgin Islands; Cayman Islands; Cuba; Domonican Republic; Grenada; Guadeloupe; Haiti; Jamaica; Martinique; Montserrat; Puerto Rico; Bonaire, Sint Eustatius and Saba; Saint Kitts and Nevis; Saint Lucia; Saint Vincent and the, and Grenadines; Trinidad and Tobago; Turks and Caicos Islands; Virgin Islands, U.S.Grenadines;
C	East Asia	Japan; North Korea; South Korea
D	East Asia	China Mainland; Taiwan
E	South East Asia	Cambodia; Indonesia; Laos; Malaysia; Myanmar; Philippines; Singapore; Thailand; Timor-Leste; Vietnam
F	South Asia	Bangladesh; India; Sri Lanka

The table lists specific countries included in each of the six panels of Fig. 1. Only countries/regions with populations exposed to tropical cyclones are noted in the table.

Extended Data Table 2 | Sensitivity tests of the RDI ratio using different wind modelling approaches

Country / Region	Quad-by-Quad	Quad-by-Quad-85	C15+LC12
Portugal	2.01	2.01	0.90
Costa Rica	1.80	1.78	1.78
Canada	1.47	1.43	1.50
South Korea	1.45	1.43	0.87
Nicaragua	1.42	1.43	1.44
Cuba	1.34	1.31	1.29
Australia	1.32	1.44	1.31
Guatemala	1.25	1.27	1.28
Mexico	1.24	1.19	1.21
Ireland	1.20	1.22	1.08
Laos	1.17	1.15	1.15
Honduras	1.16	1.33	1.33
Haiti	1.14	1.13	1.12
Puerto Rico	1.13	1.13	1.13
Myanmar	1.13	1.11	1.15
Vietnam	1.12	1.23	1.24
North Korea	1.11	1.11	0.99
Somalia	1.09	1.08	NA
Oman	1.09	1.06	1.07
Bangladesh	1.04	1.02	1.10
China	1.01	1.00	0.97
Mozambique	0.95	0.93	0.93
India	0.91	0.89	1.01
Madagascar	0.88	0.88	0.87
United States	0.79	0.76	0.81
Jamaica	0.75	0.73	0.80
Philippines	0.74	0.87	0.80
Japan	0.65	0.62	0.57
Taiwan	0.49	0.49	0.49

The population-weighted RDI ratio (the RDI among those exposed to tropical cyclones divided by the RDI among those unexposed) calculated using three different wind modelling approaches in all affected countries/regions. Quad-by-Quad is our primary approach used in Fig. 4, whereas the RDI ratio estimated using the Quad-by-Quad-85 and C15+LC12 approaches are shown for comparison (more details in the 'Other wind modelling approaches for sensitivity tests' section). This table is used to generate Fig. 4 and Extended Data Fig. 6a,b.